Enhancing the Resistive Switching Performance in a Physically Transient Memristor by Doping MoS_2 Quantum Dots

Yizhen Li,[1,2] Xinhui Zhao,[1,2] Ke Chang,[1,2] Yiru Niu,[1,2] Xinna Yu,[1,2] and Hui Wang[1,2,*]

[1] *State Key Laboratory of Advanced Optical Communication Systems and Networks, School of Physics and Astronomy, Shanghai Jiao Tong University, 800 Dongchuan Road, Shanghai 200240, People's Republic of China*

[2] *Key Laboratory for Thin Film and Microfabrication Technology of the Ministry of Education, Research Institute of Micro/Nano Science and Technology, Shanghai Jiao Tong University, 800 Dongchuan Road, Shanghai 200240, People's Republic of China*

(Received 28 October 2021; revised 30 December 2021; accepted 17 February 2022; published 2 March 2022)

Resistive random-access memory has attracted tremendous attention and numerous investigations as a promising next-generation nonvolatile memory device to address the physical limits of flash memory. Particularly, physically transient resistive switching memory is intensively researched for its degradable and environmentally friendly characteristics. Zinc oxide (ZnO), as a low-cost biocompatible and biodegradable material, has been widely used in the dielectric layer, yet many previous studies on ZnO-based memory devices show unsatisfactory switching properties. In this work, MoS_2 quantum dots (QDs) are added between the W bottom electrode and ZnO insulator by spin coating (W/MoS_2 QD/ZnO/Ag) to improve its resistive switching behavior. The modified device exhibits distinctly better properties, including more-uniform switching parameters (low- and high-resistance states, V_{set}, V_{reset}), ultralow threshold voltages, and steady retention. Moreover, we transfer the device onto polyvinyl alcohol substrate, making it fully degradable, and it is completely dissolved in phosphate-buffered solution after 40 min. These results indicate that the MoS_2 QD–optimized transient resistive switching memory shows great potential in green electronics, implantable biomedical devices, and secure information-storage applications.

DOI: 10.1103/PhysRevApplied.17.034007

I. INTRODUCTION

In the big-data era, resistive random-access memory (RRAM) is universally considered as a potential next-generation memory device, as it not only stores and processes information but also displays superior performance characteristics compared with traditional memristors, including its nonvolatility, nanoscale size, low energy consumption, and higher endurance [1]. However, with the rapid growth of consumer electronics use and discarding, electronic waste has become a major 21st-century issue that enlarges landfill space and poses environmental threats [2–4]. Consequently, transient electronic devices like transient memristors are imminently desired on account of their biodegradability after a demanded period of operation, leaving no or minimum impact on the surrounding environment [5–7]. In addition to being eco-friendly, physically transient memory devices have a variety of applications, such as secure information storage that eliminates data after use and biomedical devices that are implantable and nontoxic. [8–12].

Among numerous studied semiconductors in the top electrode (TE)-semiconductor-bottom electrode (BE)–structured transient resistive switching (RS) memory devices, ZnO exhibits strongly competitive properties, such as low cost, wide band gap of 3.37 eV, outstanding chemical stability, high electron mobility, transparency, biocompatibility, and biodegradability [13–17]. Nevertheless, in ZnO-based RS memory devices, often zinc interstitial and oxygen vacancy defects are formed in the fabricated ZnO thin film, and these defects may lead to poor switching behavior [18]. In an effort to enhance the RS properties of ZnO-based memristors, many attempts have been made, including stacking multiple metal electrodes, embedding different metal oxides, doping various elements, and manipulating growth deposition; however, nearly all past research results show a large set voltage of >1 V, a reset voltage of <-0.5 V, and poor endurance of 20–100 cycles [18–27]. Moreover, quantum dots (QDs) can regulate the growth of conductive filaments by modifying the surrounding electric field, resulting in a reinforced resistive switching performance; nevertheless, a convenient and efficient refinement method of doping MoS_2 QDs in a transient ZnO RS device has rarely been researched or reported.

In our work, MoS_2 QDs, a bioavailable, biocompatible, and biodegradable nanomaterial that possesses unique structural and physical features [28], are spin coated on

*huiwang@sjtu.edu.cn

TABLE I. Comparison of our Ag/MoS_2 QD/ZnO/W device and other ZnO-based RRAM.

No	Structure	V_{set} (V)	V_{reset} (V)	Endurance (cycles)	*On*:*off* ratio (times)	Ref.
1	Ag/MoS_2 QD/ZnO/W (our device)	0.12	−0.25	>200	$>10^2$	
2	Ag/ZnO/Pt	0.8	−0.4	40	10^2	[29]
3	Cu/ZnO/ITO	2.6	0.6	300	>20	[30]
4	Pt/ZnO/Pt	1.5	0.5	200	58	[31]
5	Cu/ZnO/Pt	1.5	−0.5	100	$>10^2$	[32]
6	Ag/GZO/ZnO/Pt	0.4	−0.55	40	10^3	[33]
7	Pt/ZnO/ZrO_2/Pt	3	−4	100	5	[34]
8	Pt/$(ZnO/Ti/ZnO)_{1-4}$/ITO	2	−2.5	320	10^3	[35]
9	Pt/Ga_2O_3/ZnO/Pt	1.7	−1.4	20	10^2	[36]
10	Ag/CeO_2/ZnO/NSTO	2	−5	100	540	[37]
11	Pt/ZnO/$Ag_{0.2}$-$Al_{0.8}$/Al	2	0.3	200	$>10^2$	[38]
12	Pt/TiO_x/ZnO/n^+-Si	2	0.5	>50	$>10^2$	[39]
13	Pt/Mn : ZnO/Si	20	−20	4500	10^3	[40]
14	Al/ZnO : Cu/Pt	2	0.5	450	470	[41]
15	Cu/ZnO : Mn/Pt	1.2	−0.6	65	10^3	[42]
16	Pt/Co : ZnO/Pt	1.5	−1	300	10^2	[22]

a W BE. Thus, we fabricate a RS memory device with the simple construction of W/MoS_2 QD/ZnO/Ag. This device demonstrates particularly remarkable RS properties, with V_{set} as low as 0.12 V, V_{reset} of −0.25 V, good endurance of more than 200 cycles, robust retention of 10^4 s, and an *on*:*off* ratio of $>10^2$. Our device possesses threshold voltages more than 2 times lower and endurance more than 2 times better than those published in the literature (a comparison of our device and other ZnO-based RRAM is shown in Table I). More significantly, compared with the W/ZnO/Ag device we make, it manifests evidently lower threshold voltages and distinctly more uniformly distributed RS parameters [V_{set}, V_{reset}, high-resistance state (HRS), and low-resistance state (LRS)]; therefore, we obtain a superior RS memory device with reduced energy consumption and reinforced stability and reliability. In addition, a RS conduction-mechanism model is established to illustrate how resistive switching works and how MoS_2 QDs regulate RS behavior. It is found that MoS_2 QDs distort the electric field near the W bottom electrode; as a consequence, the conductive metal filaments, the formation and rupture of which are responsible for resistive switching, tend to grow from the MoS_2 QDs, decreasing the randomness of the memory device [40,43–45]. After transferring the device onto soluble polyvinyl alcohol (PVA) substrate, a totally degradable memristor is achieved; its electrical measurements indicate no marked change. We verify the transient characteristic by immersing it in phosphate-buffered solution (PBS), and it can be completely dissolved at room temperature after 40 min.

II. FABRICATION AND METHODS

Two types of memristors were fabricated for comparison in an effort to analyze the effects of MoS_2 quantum dots: W/ZnO/Ag and W/MoS_2 QD/ZnO/Ag. The W/MoS_2 QD/ZnO/Ag device is prepared as follows. First, a 100-nm W thin film is deposited on a silicon substrate under an Ar pressure of 0.53 Pa with direct-current (dc) magnetron sputtering. MoS_2 quantum dots are spin coated on the W bottom electrode at a speed of 4000 rpm for 40 s. Then a 57-nm ZnO switching layer is deposited under an Ar pressure of 0.86 Pa with radio-frequency (rf) sputtering. Finally, a 20-nm Ag top electrode layer is deposited with a mask template under an Ar pressure of 0.55 Pa with dc sputtering. A schematic of this device is illustrated in Fig. 1(a). Furthermore, to prepare the PVA substrate, we dissolve 15 wt % PVA powder (molecular weight approximately 31 000, 87%–90% hydrolyzed) in deionized water and stir the solution at 70 °C for 12 h, after which time it is drop cast in a culture dish and dried at 90 °C for 24 h. Then the fabricated device is transferred onto PVA substrate with thermal release tape. Thus, a fully degradable memory device is completed.

Electrical characteristics measurements are carried out with a Keithley 4200 SCS parameter analyzer in a Lake Shore Cryotronics TTPX probe station, and voltage cycles of $0 \rightarrow 2 \rightarrow 0 \rightarrow -2 \rightarrow 0$ V are applied to the TE; the BE is earthed. Scanning electron microscopy (SEM) testing reveals the cross-section image of the device and a sandwich structure of W(100 nm)/ZnO(57 nm)/Ag(20 nm) is clearly detected [Fig. 1(b)]. Notably, due to the 4–5-nm scale of QDs, they are not prominent in SEM cross-section scanning. Atomic force microscopy (AFM) is used to examine the surface morphology of MoS_2 QDs. Figure 1(c) showcases the AFM image of the W bottom electrode with MoS_2 QDs, and Fig. 1(d) is the AFM scanning result along the line in Fig. 1(c). The height of QDs is about 4 nm, and the distribution density is about 15 dots/μm^2. Transmission electron microscopy (TEM) is performed to

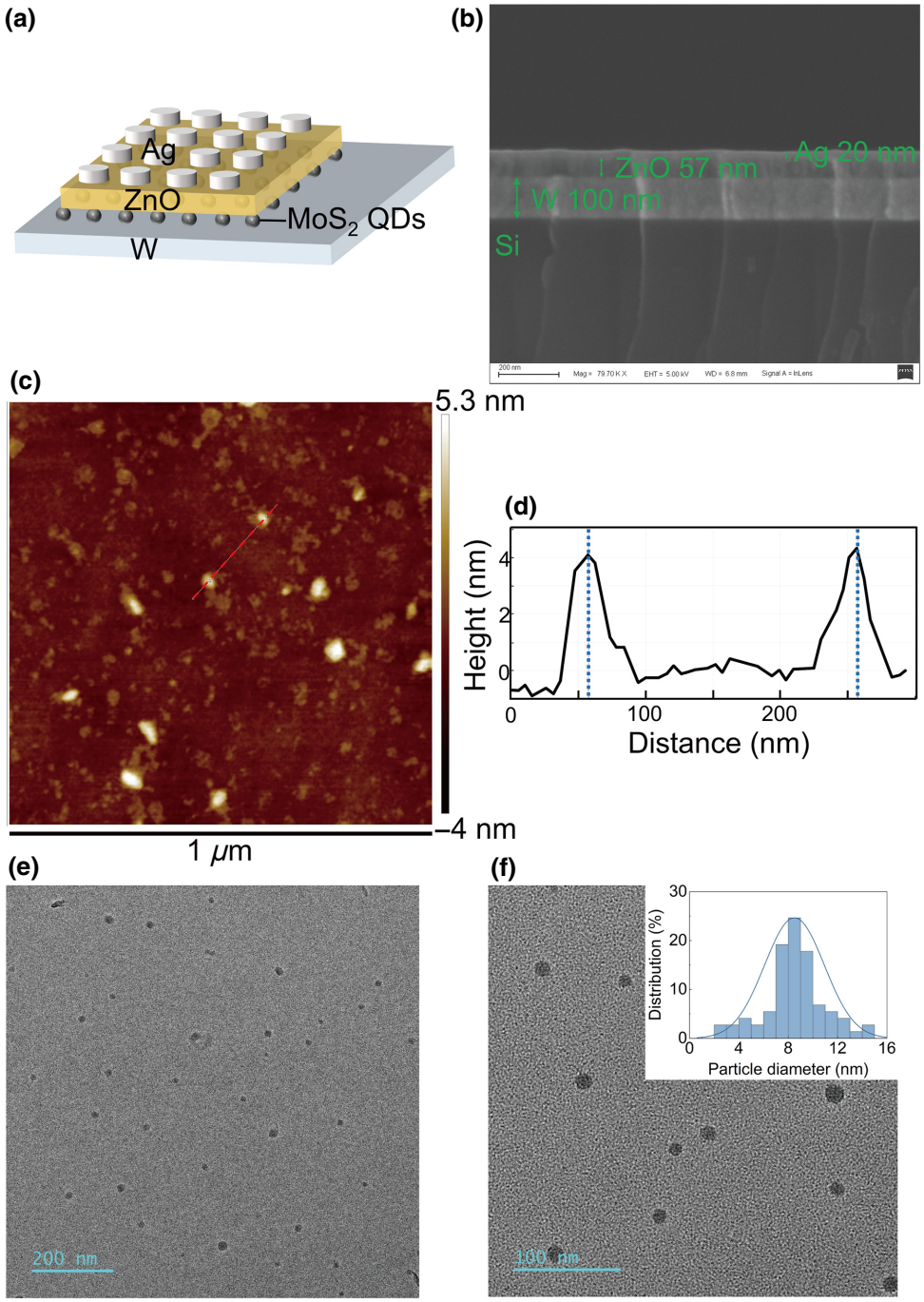

FIG. 1. (a) Schematic diagram of the structure of W/MoS_2 QD/ZnO/Ag device. (b) Cross-section SEM image of the device. (c) AFM image of MoS_2 QDs spin coated on the W bottom electrode. (d) AFM scanning result along the straight line in (c). (e) TEM image of MoS_2 QDs. (f) TEM image of MoS_2 QDs on a smaller scale. Inset is the particle diameter distribution of MoS_2 QDs.

analyze the lateral particle size of MoS_2 QDs. Figures 1(e) and 1(f) are the TEM images of MoS_2 QDs at different scales and the distribution of granule diameters. We can observe that the grain diameter of MoS_2 QDs is around 8 nm. With a transverse diameter of 8 nm and a longitudinal height of 4 nm, the MoS_2 QD takes a hemispherical shape on the bottom electrode.

III. RESULTS AND DISCUSSION

A series of electrical measurements are performed to reveal the properties of the devices. Figures 2(a) and 2(b) demonstrate the switching behaviors of W/ZnO/Ag and W/MoS_2 QD/ZnO/Ag devices. Both devices exhibit nonvolatile bipolar resistive switching behavior without a forming process. First, a positive sweeping voltage of 0 to 2 V with a compliance current of 1 mA is applied to the device, and it switches from a HRS to a LRS, identified as the set process; then by applying a negative sweeping voltage of 0 to −2 V, the device switches from LRS to HRS, known as the reset process. In comparison with W/ZnO/Ag, W/MoS_2 QD/ZnO/Ag displays distinctly better uniformity, with an ultralow set voltage (V_{set}) ranging from 0.12 to 0.24 V and a reset voltage (V_{reset})

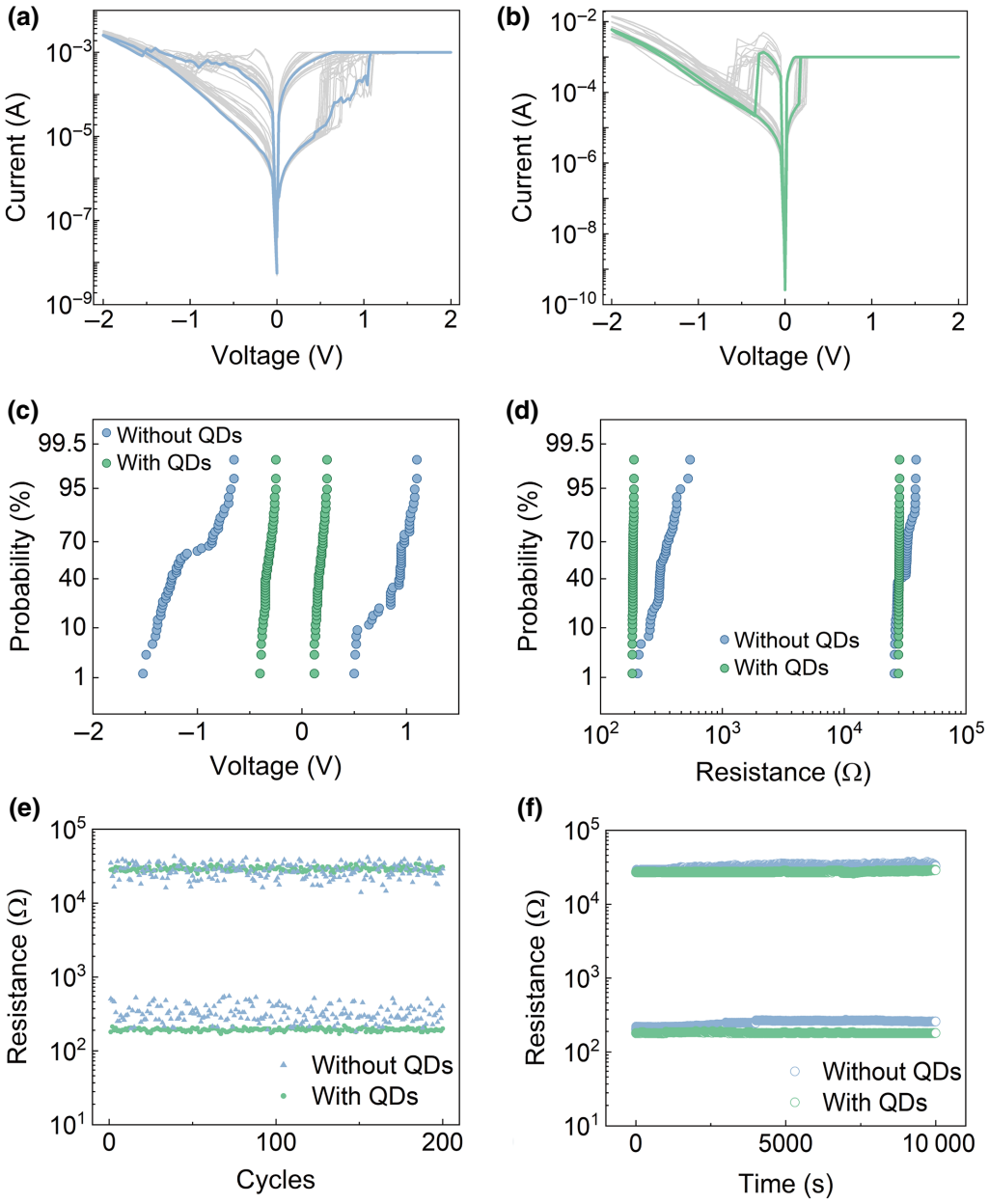

FIG. 2. *I-V* characteristics of the W/ZnO/Ag device (a) without MoS_2 QDs and (b) with MoS_2 QDs. (c) Statistical cumulative probabilities of V_{set} and V_{reset} and (d) LRS and HRS of the two devices of 50 cycles. (e) Endurance performance and (f) retention performance of the two devices with a read voltage of 0.1 V.

ranging from −0.25 to −0.4 V, whereas the set voltage of the device without MoS_2 QDs ranges from 0.5 to 1.1 V and its reset voltage is distributed in the range of −0.65 to −1.52 V. The modified device demonstrates a more than 4 times lower set voltage and a more than 2 times lower reset voltage, which substantially reduces energy consumption and simplifies peripheral circuits. Figure 2(c) showcases the statistical cumulative probability of switching voltages of the two devices for 50 sweeping cycles. It visually confirms that threshold voltages of the device with QDs are more centralized around a smaller value, while those of the device without QDs vary over a large scale. As illustrated in Fig. 2(d), the resistance-state distribution of the QD-doped device also exhibits higher uniformity with only slight fluctuations. Its LRS is distributed between 180 and 200 Ω, and the HRS is located between 2.7×10^4 and 3×10^4 Ω in contrast, the LRS of the device without QDs fluctuates in the range of 200 to 540 Ω, and the HRS fluctuates from 2.5×10^4 to 3.8×10^4 Ω. Figure 2(e) depicts a comparison of endurance performance between the two tested devices for 200 cycles. It is notable that, besides enhanced resistance stability from cycle to cycle, the device with MoS_2 QDs has a larger *on*:*off* ratio of $>10^2$ because of its lower LRS compared with the device without QDs, which offers an enlarged memory window for preferable data-storage capacity. Moreover, the optimized device is able to endure voltage sweeps of more than 200 cycles without experiencing any marked degradation, indicating its excellent reliability. Retention is another significant indicator in evaluating the performance of

memory devices. Figure 2(f) illustrates the retention characteristics of the two devices measured with a read voltage of 0.1 V. The modified device demonstrates nonvolatility and robust retention with no evident variation for as long as 10^4 s, whereas the device without QDs experiences upward fluctuations as time increases, especially in its LRS. These results reveal that the device with MoS_2 QDs presents lower switching voltages and superb stability and reliability, making it suitable for nonvolatile memory applications.

To explore the conduction mechanism of the W/MoS_2 QD/ZnO/Ag RS memory device, double-logarithmic plots of *I-V* curves in the HRS and LRS are redrawn, and their corresponding linear fittings are also analyzed. Figures 3(a)–3(f) demonstrate double-logarithmic plots of *I-V* curves from three different devices, and we can conclude that there are two linear sections in the HRS: the first region of HRS shows a consistent linear relationship between I and V, with a slope of about one, and the second region displays a linear relationship with a slope of about two; these slopes agree well with the ohmic law and space-charge-limited current (SCLC) model ($I \propto V^2$), respectively. As for the LRS, the double-logarithmic *I-V* curves manifest a consistent linear relationship between I and V. The slopes of linear fitting lines are approximately one, which indicates that the LRS is dominated by ohmic conduction and conductive channels form in the ZnO layer.

The conduction mechanism of RS devices structured as inert metal electrode-oxide-active metal electrode has been comprehensively studied over the years. It is widely acknowledged that the conductive channels responsible for the LRS are conductive metal filaments, and their formation and rupture result in the resistive switching behavior [19,26,44,46]. In our experiments, a contrast device structured as W/ZnO/W is fabricated to investigate the conductive channels. No resistive switching behavior is detected in our electrical tests on this device, and its *I-V* curve with a positive voltage sweep of 0–10 V is illustrated in Fig. 3(c), verifying that Ag conductive filaments account for RS behavior in our memristors. Combined with the theory of metal redox reactions, we plot a schematic diagram of the RS process to explain the underlying mechanism, shown in Figs. 4(a)–4(d). First, a positive voltage is applied to the top electrode and Ag easily oxides into Ag^+ ($Ag \rightarrow Ag^+ + e^-$) at the Ag/ZnO interface, as is shown in Fig. 4(a). These Ag^+ ions migrate towards the cathode in the ZnO layer under the influence of an electric field and eventually reach the cathode. Then through a reduction reaction with electrons produced by the cathode, Ag^+ ions are converted back into Ag atoms ($Ag^+ + e^- \rightarrow Ag$), as depicted in Fig. 4(b). Finally, as Fig. 4(c) illustrates, with the gradual accumulation of Ag atoms on the BE, a metal filament bridge is constructed between two electrodes. The formation of a highly conductive Ag filament bridge causes the device to switch from the HRS to the LRS. As for the reset process, after a negative voltage is applied to the TE, conductive metal filaments rupture under the effect of a reverse electric field coupled with Joule heating, as plotted in Fig. 4(d), and it results in the device transforming back to the HRS.

To further interpret how MoS_2 QDs regulate RS behavior in our device, a formation model of Ag conductive filaments during the set process is established, which is displayed in Figs. 4(e) and 4(f). MoS_2 QDs regulate Ag conductive filament growth by altering the electric field distribution. The intensity of the electric field around QDs is distinctly higher than that in other regions. On the basis of our AFM and TEM results [Figs. 1(c) and 1(f)], we simulate the electric field distribution around a MoS_2 quantum dot with MATLAB, as demonstrated in Fig. 4(g). The QD is a hemisphere on the BE and a semicircle in two dimensions. The simulated voltage is 0–1 V. For the device without QDs, the electric field is distributed homogeneously in the ZnO layer; however, the electric field becomes inhomogeneous with QDs, and we find that equipotential lines converge around the QD, indicating that the QD significantly enhances its surrounding electric field. On account of the enhanced localized electric field, Ag^+ cations tend to cluster around QDs and once the Ag nucleus takes shape, it obtains an extremely high electrochemical deposition rate of Ag atoms, owing to an even stronger electric field [47–49]. To elaborate on this, combining the Arrhenius equation with transition-state theory, the mechanism rate is expressed as [50]

$$\Gamma = \nu \exp(-E_A/kT), \tag{1}$$

in which ν is a fixed vibration factor, E_A is the activation energy, k is the Boltzmann constant, and T is the temperature. E_A is regulable by the local electric field [51]:

$$E'_A = E_A - \frac{qd\epsilon_{\text{local}}}{2} - \frac{\Delta E}{2}, \tag{2}$$

where E'_A is the modified activation energy, q is the particle charge, d is the distance, ϵ_{local} is the local electric field, and ΔE is the energy gap. The probability of state transition, P, during time t is [51]

$$P = 1 - \exp(-\Gamma t). \tag{3}$$

From above, we can deduce that a higher ϵ_{local} leads to a lower E'_A; a higher Γ; and, consequently, a higher P, meaning that a higher localized electric field decreases the activation energy needed and increases the state-transition probability.

Thus, Ag atoms gradually accumulate to reach the TE, forming a conductive filament specifically on the QD, as illustrated in Fig. 4(f). On the contrary, shown in Fig. 4(e), unguided Ag atoms are deposited randomly on the BE,

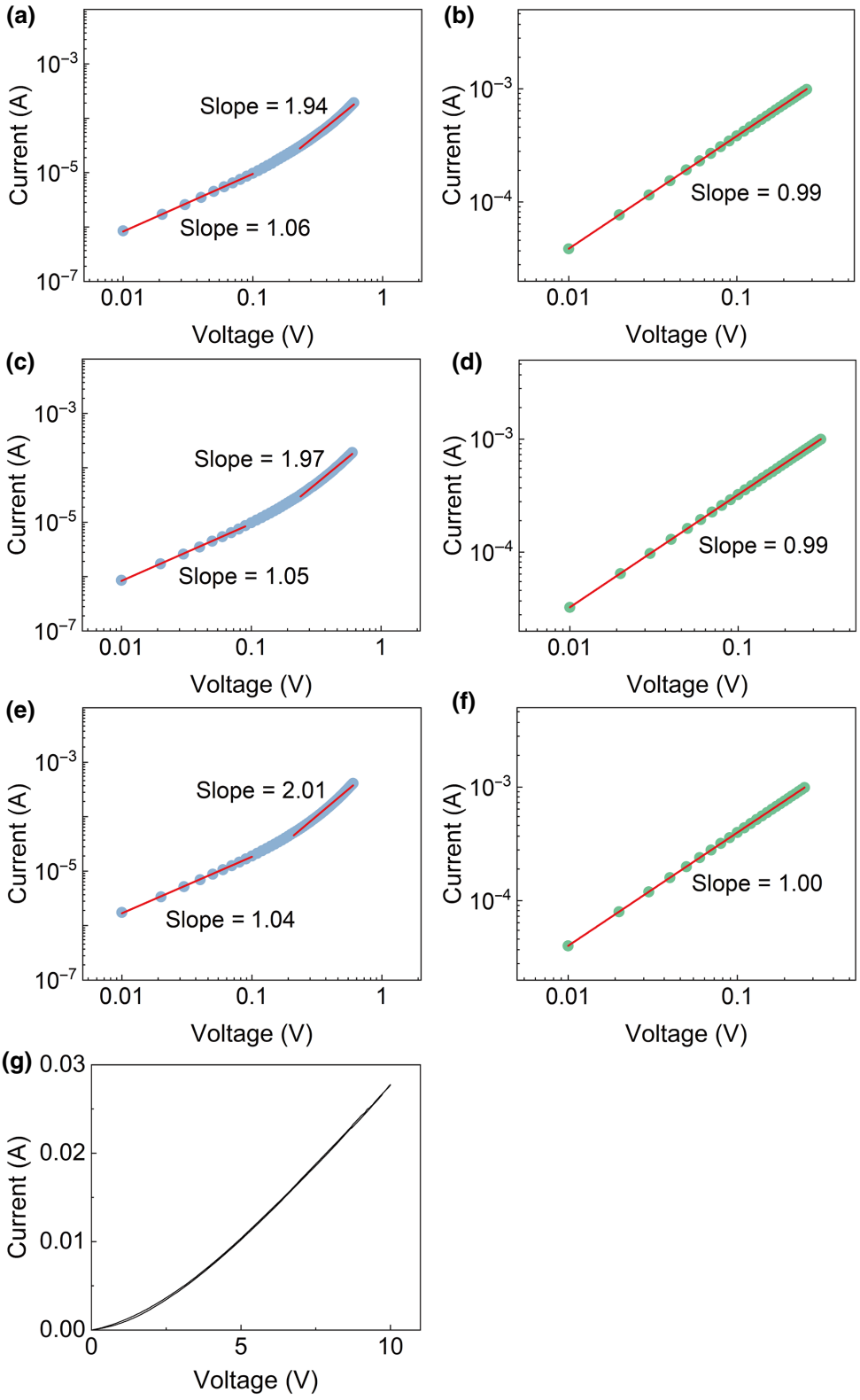

FIG. 3. Double-logarithmic plots of *I-V* curves in HRS and LRS from different devices and their linear fittings. (a) HRS and (b) LRS from device 1. (c) HRS and (d) LRS from device 2. (e) HRS and (f) LRS from device 3. (g) *I-V* curve of W/ZnO/W device.

and Ag filaments grow to have various shapes due to the irregular migration of Ag^+ ions. Hence, in the device without QDs, different numbers and shapes of conductive filaments form during voltage-sweeping cycles, leading to a scattered distribution of switching parameters (LRS, HRS, V_{set}, V_{reset}) [48]. Notably, multistep set and reset processes are commonly observed in the RS behavior of the device without QDs [Fig. 2(a)], mainly because

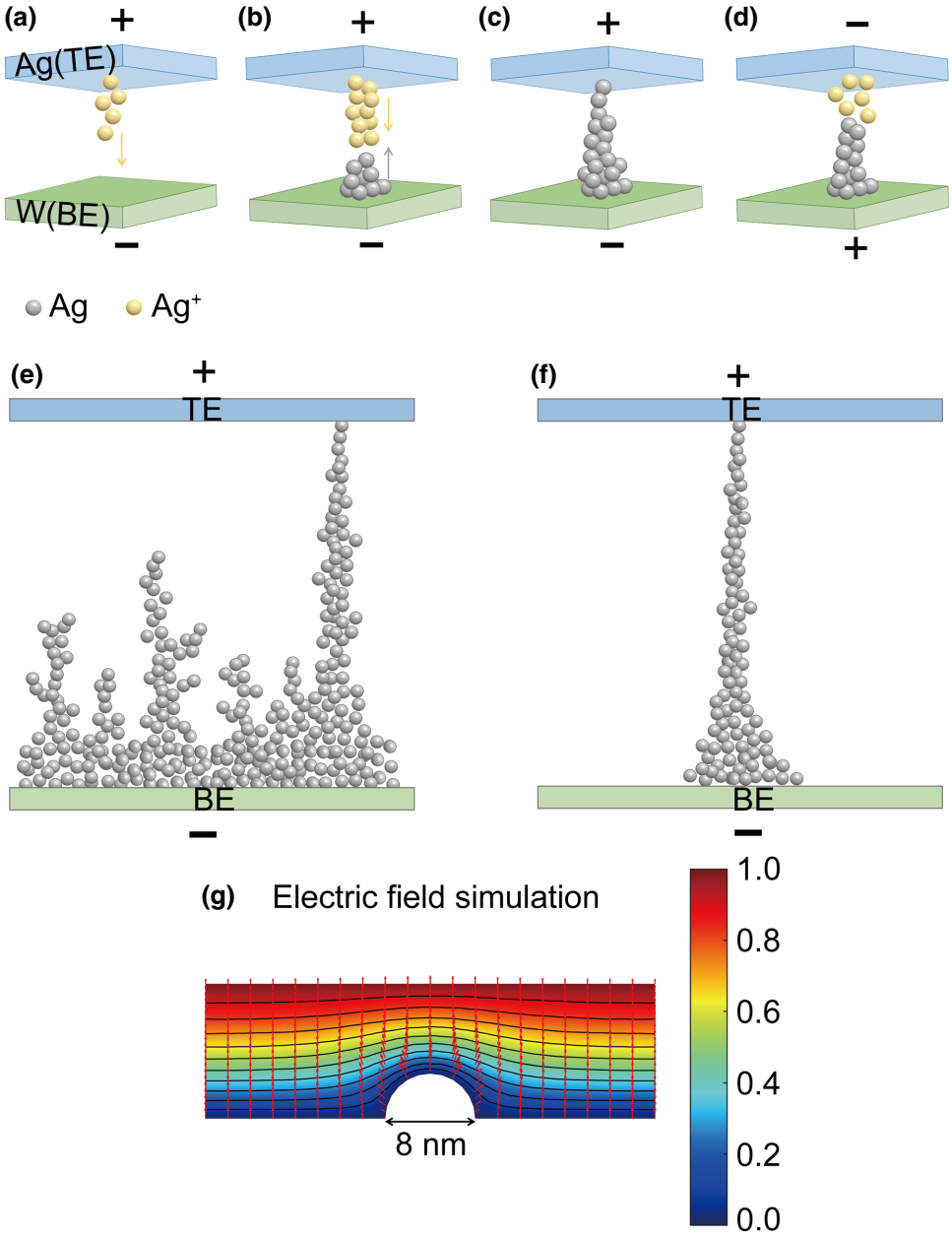

FIG. 4. Schematic diagram of RS mechanism in our memory devices: (a) Oxidation of Ag to Ag^+ at Ag/ZnO interface. (b) Migration of Ag^+ ions and reduction reaction at the bottom electrode. (c) Formation of Ag conductive filament. (d) Rupture of Ag conductive filament under a reverse voltage. (e) Schematic diagram of Ag filament growth in device without MoS_2 QDs. (f) Schematic diagram of Ag filament growth in device with MoS_2 QDs. (g) Electric field simulation with MATLAB in ZnO layer from 0 to 1 V around a MoS_2 quantum dot and equipotential lines are also illustrated.

ruleless intrinsic zinc-interstitial and oxygen-vacancy defects are created during ZnO sputtering [52]. However, with the guidance of MoS_2 QDs, multistep set and reset processes are eliminated [Fig. 2(b)] and the previously poor switching quality is improved. Additionally, the retention characteristic is fundamentally dominated by surface diffusion of conductive atoms [53]. After the voltage is removed from the device, the diffusion rate of Ag atoms is superlow at room temperature, contributing to a long and steady resistance retention. Consequently, by modifying an adjacent electric field, MoS_2 QDs control the growth of Ag conductive filaments, generating more ordered and stabilized conductive paths in the W/MoS_2 QD/ZnO/Ag device. These paths lead to ultralow switching voltages, lower LRS, and more uniformly distributed switching parameters from cycle to cycle.

Additionally, after transferring the W/MoS_2 QD/ZnO/Ag device onto the PVA substrate that we prepare, we obtain a fully transient memory device, as shown in Fig. 5(b). In terms of switching voltages, I-V curves, and uniformity, its electrical properties [Fig. 5(a)] demonstrate no marked difference from the original device on silicon substrate. We immerse the device in PBS (pH = 7.4) to investigate its transient characteristics. Figures 5(b)–5(f) are the dissolution images of the device soaked in PBS at room temperature after 1, 5, 10, 20, and 40 min. The resistive switching part completely dissolves in only

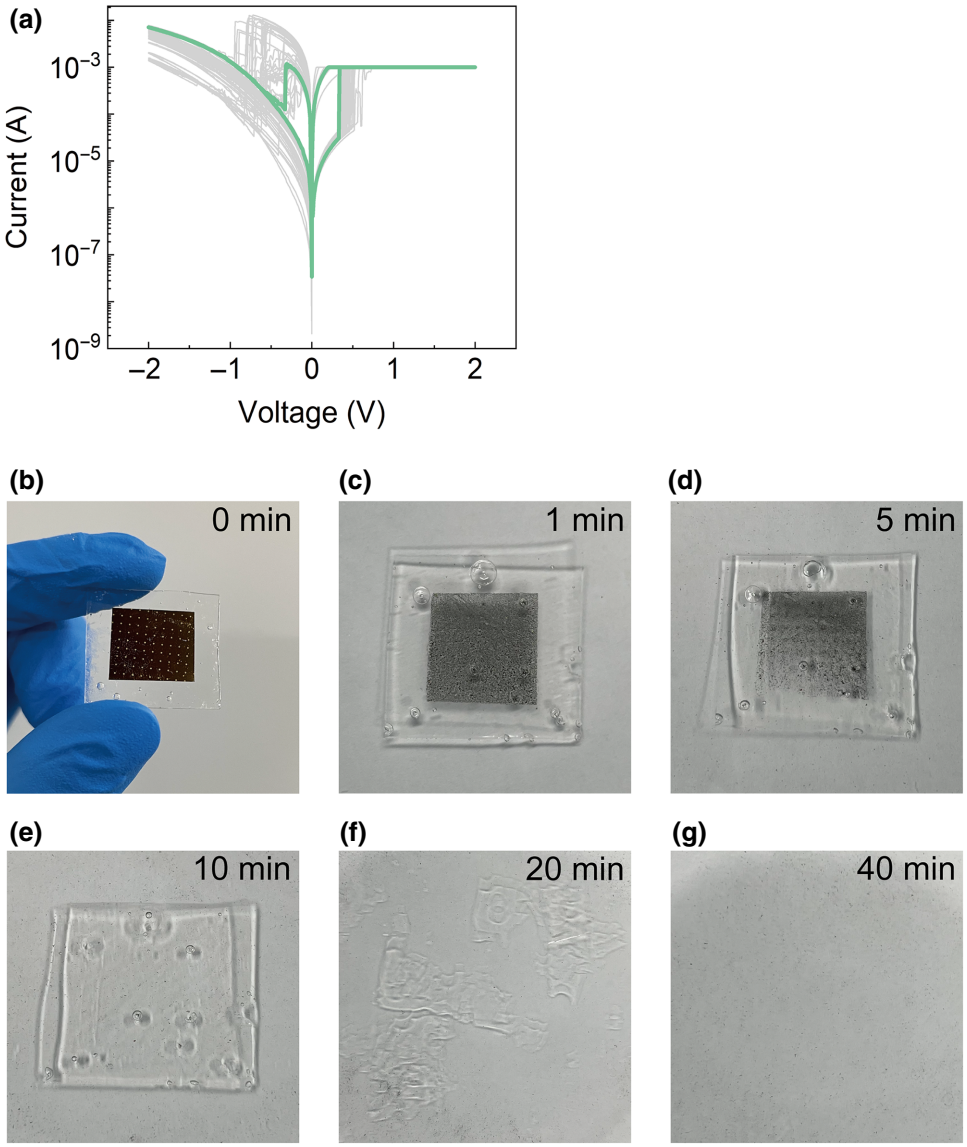

FIG. 5. (a) *I-V* characteristics of the W/MoS_2 QD/ZnO/Ag device on PVA substrate. Fully transient property of the device on PVA substrate. (b) Device transferred onto PVA substrate. (c) Image of the device immersed in PBS at room temperature after 1 min, (d) 5 min, (e) 10 min, (f) 20 min, and (g) 40 min.

10 min and, after 40 min, the PVA substrate is also fully dissolved in PBS. Specifically, the hydrolysis of W is based on the reaction $2W + 2H_2O + 3O_2 \rightarrow 2H_2WO_4$, and the hydrolysis of ZnO occurs through the reaction $ZnO + H_2O \rightarrow Zn^{2+} + 2OH^-$, turning into much more diffluent substances [54,55]. The nanoscale Ag top electrode and MoS_2 QDs are also proven to be degradable in water [28,56]. The MoS_2 quantum dot is a transition-metal-dichalcogenide nanomaterial that is nontoxic, biocompatible, and environmentally friendly, the nontoxicity of which has been studied and demonstrated by many research groups [57,58]. Ag nanoparticles of lower concentration are nontoxic, while higher concentrations of Ag nanoparticles and Ag^+ can trigger serious environmental issues [59–61]. Nevertheless, Ag nanoparticles can be recovered and recycled from solutions, which largely relieves the environmental stress and facilitates sustainability [62,63]. Therefore, the rapid dissolution property and environmental friendliness make our device appropriate for physically transient electronics applications.

IV. CONCLUSION

We propose a fully transient MoS_2 QD–doped resistive switching memory device on PVA substrate. MoS_2 QDs enable Ag conductive filaments to grow in a controlled manner by modifying the surrounding electric field. Compared with the device without QDs, the optimized device displays more centralized RS parameters, including resistance states and threshold voltages, ultralow set and reset voltages, and more stable retention. Additionally, the device on PVA substrate is fully dissolved in PBS after 40 min at room temperature. This easily fabricated RS device showcases high performance; low power consumption; and, thus, tremendous potential in physically transient RS memory application.

ACKNOWLEDGMENTS

We acknowledge financial support from the National Natural Science Foundation of China under Grants No. 11874041, No. 61574090, No. 11374214, and No. 10974135. The authors would like to thank N. Han from Shiyanjia Lab [64]for the AFM and TEM analysis and Ms. W. Jiang from Advanced Electronic Materials and Devices (AEMD) of Shanghai Jiao Tong University for the SEM analysis.

[1] J. J. Yang, D. B. Strukov, and D. R. Stewart, Memristive devices for computing, Nat. Nanotechnol. **8**, 13 (2013).

[2] W. Hu, B. Yang, Y. Zhang, and Y. She, Recent progress in physically transient resistive switching memory, J. Mater. Chem. C **8**, 14695 (2020).

[3] X. Ji, L. Song, S. Zhong, Y. Jiang, K. G. Lim, C. Wang, and R. Zhao, Biodegradable and flexible resistive memory for transient electronics, J. Phys. Chem. C **122**, 16909 (2018).

[4] K. K. Fu, Z. Wang, J. Dai, M. Carter, and L. Hu, Transient electronics: Materials and devices, Chem. Mater. **28**, 3527 (2016).

[5] C. Dagdeviren, S. W. Hwang, Y. Su, S. Kim, H. Cheng, O. Gur, R. Haney, F. G. Omenetto, Y. Huang, and J. A. Rogers, Transient, biocompatible electronics and energy harvesters based on ZnO, Small **9**, 3398 (2013).

[6] S. W. Hwang, *et al.*, A physically transient form of silicon electronics, Science **337**, 1640 (2012).

[7] M. Irimia-Vladu, P. A. Troshin, M. Reisinger, L. Shmygleva, Y. Kanbur, G. Schwabegger, M. Bodea, R. Schwödiauer, A. Mumyatov, J. W. Fergus, V. F. Razumov, H. Sitter, N. S. Sariciftci, and S. Bauer, Biocompatible and biodegradable materials for organic field-effect transistors, Adv. Funct. Mater. **20**, 4069 (2010).

[8] B. Dang, Q. Wu, F. Song, J. Sun, M. Yang, X. Ma, H. Wang, and Y. Hao, A bio-inspired physically transient/biodegradable synapse for security neuromorphic computing based on memristors, Nanoscale **10**, 20089 (2018).

[9] C. J. Bettinger and Z. Bao, Organic thin-film transistors fabricated on resorbable biomaterial substrates, Adv. Mater. **22**, 651 (2010).

[10] C. J. Bettinger and Z. Bao, Biomaterials-Based organic electronic devices, Polym. Int. **59**, 563 (2010).

[11] D. H. Kim, Y. S. Kim, J. Amsden, B. Panilaitis, D. L. Kaplan, F. G. Omenetto, M. R. Zakin, and J. A. Rogers, Silicon electronics on silk as a path to bioresorbable, implantable devices, Appl. Phys. Lett. **95**, 133701 (2009).

[12] N. R. Hosseini and J. S. Lee, Biocompatible and flexible chitosan-based resistive switching memory with magnesium electrodes, Adv. Funct. Mater. **25**, 5586 (2015).

[13] F. Song, H. Wang, J. Sun, H. Gao, S. Wu, M. Yang, X. Ma, and Y. Hao, ZnO-Based physically transient and bioresorbable memory on silk protein, IEEE Electron Device Lett. **39**, 31 (2018).

[14] J. Zhou, N. Xu, and Z. L. Wang, Dissolving behavior and stability of ZnO wires in biofluids: A study on biodegradability and biocompatibility of ZnO nanostructures, Adv. Mater. **18**, 2432 (2006).

[15] R. L. Hoffman, B. J. Norris, and J. F. Wager, ZnO-Based transparent thin-film transistors, Appl. Phys. Lett. **82**, 733 (2003).

[16] C. A. David, J. Galceran, C. Rey-Castro, J. Puy, E. Companys, J. Salvador, J. Monné, R. Wallace, and A. Vakourov, Dissolution kinetics and solubility of ZnO nanoparticles followed by AGNES, J. Phys. Chem. C **116**, 11758 (2012).

[17] Ü Özgür, Y. I. Alivov, C. Liu, A. Teke, M. A. Reshchikov, S. Doğan, V. Avrutin, S. J. Cho, and H. Morkoç, A comprehensive review of ZnO materials and devices, J. Appl. Phys. **98**, 041301 (2005).

[18] F. M. Simanjuntak, D. Panda, K. H. Wei, and T. Y. Tseng, Status and prospects of ZnO-based resistive switching memory devices, Nanoscale Res. Lett. **11**, 368 (2016).

[19] U. B. Isyaku, M. H. B. M. Khir, I. M. Nawi, M. A. Zakariya, and F. Zahoor, Zno based resistive random access memory device: A prospective multifunctional next-generation memory, IEEE Access **9**, 105012 (2021).

[20] S. Bae, D. S. Kim, S. Jung, W. S. Jeong, J. E. Lee, S. Cho, J. Park, and D. Byun, Bipolar switching behavior of ZnO_x thin films deposited by metalorganic chemical vapor deposition at various growth temperatures, J. Electron. Mater. **44**, 4175 (2015).

[21] X. Cao, X. Li, X. Gao, X. Liu, C. Yang, and L. Chen, Structural properties and resistive switching behaviour in Mg_xZn1_-xO alloy films grown by pulsed laser deposition, J. Phys. D. Appl. Phys. **44**, 015302 (2011).

[22] G. Chen, C. Song, C. Chen, S. Gao, F. Zeng, and F. Pan, Resistive switching and magnetic modulation in cobalt-doped ZnO, Adv. Mater. **24**, 3515 (2012).

[23] G. Chen, C. Song, and F. Pan, Improved resistive switching stability of $Pt/ZnO/CoO_x/ZnO/Pt$ structure for nonvolatile memory devices, Rare Met. **32**, 544 (2013).

[24] X. Chen, W. Hu, S. Wu, and D. Bao, Stabilizing resistive switching performances of $TiN/MgZnO/ZnO/Pt$ heterostructure memory devices by programming the proper compliance current, Appl. Phys. Lett. **104**, 043508 (2014).

[25] B. Cheng, Z. Ouyang, C. Chen, Y. Xiao, and S. Lei, Individual Zn_2SnO_4-sheathed ZnO heterostructure nanowires for efficient resistive switching memory controlled by interface states, Sci. Rep. **3**, 3249 (2013).

[26] M. Laurenti, S. Porro, C. F. Pirri, C. Ricciardi, and A. Chiolerio, Zinc oxide thin films for memristive devices: A review, Crit. Rev. Solid State Mater. Sci. **42**, 153 (2017).

[27] B. Liu, K. Chang, X. Yu, Y. Niu, X. Dong, and H. Wang, Compliance-Current Manipulation of Dual-Filament Switching in a $Ta/Ta_2O_5/In-Sn-O$ Structure with an Ultralow Power Consumption, Phys. Rev. Appl. **16**, 044050 (2021).

[28] M. Cao, R. Cai, L. Zhao, M. Guo, L. Wang, Y. Wang, L. Zhang, X. Wang, H. Yao, C. Xie, Y. Cong, Y. Guan, X. Tao, Y. Wang, S. Xu, Y. Liu, Y. Zhao, and C. Chen, Molybdenum derived from nanomaterials incorporates into molybdenum enzymes and affects their activities in vivo, Nat. Nanotechnol. **16**, 708 (2021).

[29] J. Z. Jianwei Zhao, F. L. Fengjuan Liu, J. S. Jian Sun, H. H. Haiqin Huang, Z. H. Zuofu Hu, and X. Z. Xiqing Zhang, Low power consumption bipolar resistive switching characteristics of ZnO-based memory devices, Chinese Opt. Lett. **10**, 013102 (2012).

[30] H. X. Li, D. D. Shen, W. Q. Ke, J. H. Xi, Z. Kong, and Z. G. Ji, Fabrication and characterization of transparent ZnO film based resistive switching devices, Key Eng. Mater. **609–610**, 565 (2014).

[31] Z. J. Liu, J. C. Chou, S. Y. Wei, J. Y. Gan, and T. R. Yew, Improved resistive switching of textured ZnO thin films grown on Ru electrodes, IEEE Electron Device Lett. **32**, 1728 (2011).

[32] F. Zhuge, S. Peng, C. He, X. Zhu, X. Chen, Y. Liu, and R. W. Li, Improvement of resistive switching in Cu/ZnO/Pt sandwiches by weakening the randomicity of the formation/rupture of Cu filaments, Nanotechnology **22**, 275204 (2011).

[33] J. W. Zhao, J. Sun, H. Q. Huang, F. J. Liu, Z. F. Hu, and X. Q. Zhang, Effects of ZnO buffer layer on GZO RRAM devices, Appl. Surf. Sci. **258**, 4588 (2012).

[34] Z. Xu, L. Yu, X. Xu, J. Miao, and Y. Jiang, Effect of oxide/oxide interface on polarity dependent resistive switching behavior in ZnO/ZrO_2 heterostructures, Appl. Phys. Lett. **104**, 192903 (2014).

[35] S. C. Qin, R. X. Dong, and X. L. Yan, Memristive behavior of ZnO film with embedded Ti nano-layers, Appl. Phys. A Mater. Sci. Process. **116**, 1 (2014).

[36] X. Li, J. G. Yang, H. P. Ma, Y. H. Liu, Z. G. Ji, W. Huang, X. Ou, D. W. Zhang, and H. L. Lu, Atomic layer deposition of Ga_2O_3/ZnO composite films for high-performance forming-free resistive switching memory, ACS Appl. Mater. Interfaces **12**, 30538 (2020).

[37] Y. Zhu, M. Li, H. Zhou, Z. Hu, X. Liu, and H. Liao, Improved bipolar resistive switching properties in CeO_2/ZnO stacked heterostructures, Semicond. Sci. Technol. **28**, 015023 (2013).

[38] Z. Q. Wang, H. Y. Xu, L. Zhang, X. H. Li, J. G. Ma, X. T. Zhang, and Y. C. Liu, Performance improvement of resistive switching memory achieved by enhancing local-electric-field near electromigrated Ag-nanoclusters, Nanoscale **5**, 4490 (2013).

[39] H. Li, X. Lv, J. Xi, X. Wu, Q. Mao, Q. Liu, and Z. Ji, Effects of TiO_x interlayer on resistance switching of $Pt/TiO_x/ZnO/n^+$-Si structures, Surf. Rev. Lett. **21**, 1450061 (2014).

[40] H. Y. Peng, G. P. Li, J. Y. Ye, Z. P. Wei, Z. Zhang, D. D. Wang, G. Z. Xing, and T. Wu, Electrode dependence of resistive switching in Mn-doped ZnO: Filamentary versus interfacial mechanisms, Appl. Phys. Lett. **96**, 2008 (2010).

[41] M. C. Kim, K. Y. Lim, C. O. Kim, and S. H. Choi, Effect of doping concentration on resistive switching behaviors of Cu-doped ZnO films, J. Korean Phys. Soc. **59**, 304 (2011).

[42] Y. C. Yang, F. Pan, and F. Zeng, Bipolar resistance switching in high-performance Cu/ZnO: Mn/Pt nonvolatile memories: Active region and influence of joule heating, New J. Phys. **12**, 023008 (2010).

[43] K. Chang, X. Yu, B. Liu, Y. Niu, R. Wang, P. Bao, G. Hu, and H. Wang, Quantum-Dots optimized electrode for high-stability transient memristor, IEEE Electron Device Lett. **42**, 824 (2021).

[44] X. Yu, K. Chang, A. Dong, Z. Gan, K. Jiang, Y. Ling, Y. Niu, D. Zheng, X. Dong, R. Wang, Y. Li, Z. Zhao, P. Bao, B. Liu, Y. Cao, S. Hu, and H. Wang, High-Performance resistive switching memory with embedded molybdenum disulfide quantum dots, Appl. Phys. Lett. **118**, 172104 (2021).

[45] W. Y. Chang, Y. C. Lai, T. B. Wu, S. F. Wang, F. Chen, and M. J. Tsai, Unipolar resistive switching characteristics of ZnO thin films for nonvolatile memory applications, Appl. Phys. Lett. **92**, 98 (2008).

[46] Y. Niu, K. Jiang, X. Dong, D. Zheng, B. Liu, and H. Wang, High performance and low power consumption resistive random access memory with $Ag/Fe_2O_3/Pt$ structure, Nanotechnology **32**, 505715 (2021).

[47] X. Yan, *et al.*, Self-assembled networked PbS distribution quantum dots for resistive switching and artificial synapse performance boost of memristors, Adv. Mater. **31**, 1805284 (2019).

[48] Q. Liu, C. Dou, Y. Wang, S. Long, W. Wang, M. Liu, M. Zhang, and J. Chen, Formation of multiple conductive filaments in the Cu/ZrO_2 : Cu/Pt device, Appl. Phys. Lett. **95**, 93 (2009).

[49] C. Schindler, G. Staikov, and R. Waser, Electrode kinetics of $Cu\text{-}SiO_2$-based resistive switching cells: Overcoming the voltage-time dilemma of electrochemical metallization memories, Appl. Phys. Lett. **94**, 072109 (2009).

[50] S. Larentis, F. Nardi, S. Balatti, D. C. Gilmer, and D. Ielmini, Resistive switching by voltage-driven Ion migration in bipolar RRAM-Part II: Modeling, IEEE Trans. Electron Devices **59**, 2468 (2012).

[51] J. Guy, G. Molas, P. Blaise, M. Bernard, A. Roule, G. Le Carval, V. Delaye, A. Toffoli, G. Ghibaudo, F. Clermidy, B. De Salvo, and L. Perniola, Investigation of forming, SET, and data retention of conductive-bridge random-access memory for stack optimization, IEEE Trans. Electron Devices **62**, 3482 (2015).

[52] H. W. Huang, C. F. Kang, F. I. Lai, H. He, S. J. Lin, and Y. L. Chueh, Stability scheme of ZnO-thin film resistive switching memory: Influence of defects by controllable oxygen pressure ratio, Nanoscale Res. Lett. **8**, 483 (2013).

[53] W. Wang, M. Wang, E. Ambrosi, A. Bricalli, M. Laudato, Z. Sun, X. Chen, and D. Ielmini, Surface diffusion-limited lifetime of silver and copper nanofilaments in resistive switching devices, Nat. Commun. **10**, 81 (2019).

[54] R. A. Reichle, K. G. McCurdy, and L. G. Hepler, Zinc hydroxide: Solubility product and hydroxy-complex stability constants from 12.5–75 °C, Can. J. Chem. **53**, 3841 (1975).

[55] L. Yin, H. Cheng, S. Mao, R. Haasch, Y. Liu, X. Xie, S. W. Hwang, H. Jain, S. K. Kang, Y. Su, R. Li, Y. Huang, and J. A. Rogers, Dissolvable metals for transient electronics, Adv. Funct. Mater. **24**, 645 (2014).

[56] J. Sun, H. Wang, Z. Wang, F. Song, Q. Zhu, B. Dang, H. Gao, M. Yang, X. Ma, and Y. Hao, Physically transient memristive synapse with short-term plasticity based

on magnesium oxide, IEEE Electron Device Lett. **40**, 706 (2019).

[57] K. Zhou, Y. Zhang, Z. Xia, and W. Wei, As-Prepared MoS_2 quantum dot as a facile fluorescent probe for long-term tracing of live cells, Nanotechnology **27**, 275101 (2016).

[58] R. Kurapati, L. Muzi, A. P. R. de Garibay, J. Russier, D. Voiry, I. A. Vacchi, M. Chhowalla, and A. Bianco, Enzymatic biodegradability of pristine and functionalized transition metal dichalcogenide MoS_2 nanosheets, Adv. Funct. Mater. **27**, 1605176 (2017).

[59] I. Kalantzi, K. Mylona, C. Toncelli, T. D. Bucheli, K. Knauer, S. A. Pergantis, P. Pitta, A. Tsiola, and M. Tsapakis, Ecotoxicity of silver nanoparticles on plankton organisms: A review, J. Nanoparticle Res. **21**, 65 (2019).

[60] M. N. Croteau, S. K. Misra, S. N. Luoma, and E. Valsami-Jones, Silver bioaccumulation dynamics in a freshwater invertebrate after aqueous and dietary exposures to nano-sized and ionic Ag, Environ. Sci. Technol. **45**, 6600 (2011).

[61] H. T. Ratte, Bioaccumulation and toxicity of silver compounds: A review, Environ. Toxicol. Chem. **18**, 89 (1999).

[62] T. Nawaz, S. Sengupta, and C. L. Yang, Silver recovery as Ag^0 nanoparticles from Ion-exchange regenerant solution using electrolysis, J. Environ. Sci. (China) **78**, 161 (2019).

[63] T. Nawaz and S. Sengupta, Silver recovery from greywater: Role of competing cations and regeneration, Sep. Purif. Technol. **176**, 145 (2017).

[64] www.shiyanjia.com